Computers and Geotechnics 159 (2023) 105498

Contents lists available at ScienceDirect

Computers and Geotechnics

journal homepage: www.elsevier.com/locate/compgeo

Surrogate-assisted uncertainty modeling of embankment settlement

Tengfei Wang [a,b], Weihang Chen [c], Taifeng Li [d,*], David P. Connolly [e], Qiang Luo [a,b,*], Kaiwen Liu [a,b], Wensheng Zhang [f]

[a] School of Civil Engineering, Southwest Jiaotong Univ, Chengdu 610031, China
[b] MOE Key Laboratory of High-Speed Railway Engineering, Southwest Jiaotong Univ, Chengdu 610031, China
[c] School of Transportation, Southeast University, Nanjing 210096, China
[d] Railway Engineering Research Institute, China Academy of Railway Sciences Co. Ltd, Beijing 100081, China
[e] School of Civil Engineering, University of Leeds, Leeds LS2 9JT, UK
[f] School of Civil and Environmental Engineering, Harbin Institute of Technology (Shenzhen), Shenzhen 518055, China

ARTICLE INFO

Keywords:
Piled embankment
Settlement
Neural network
Surrogate model
Soil property uncertainty
Structural optimization

ABSTRACT

The structural optimization of basal reinforced piled embankments is usually conducted by examining design alternatives while ignoring the inherent variability of soil properties and studying only a limited number of structural variables. As an alternative, this paper proposes a hybrid modeling framework to introduce soil property uncertainty into embankment settlement calculations. This is important because settlement is critical in the serviceability assessments considered during structural optimization. The proposed framework consists of uncertainty modeling, finite element method, surrogate modeling, and probabilistic analysis. More specifically, a neural network with Monte Carlo dropout that accounts for uncertainty is employed to correlate the soil properties which affect the long-term performance of embankments over soft clay. Next, a coupled finite element analysis is performed using two constitutive soil parameters generated by the neural network to predict post-construction settlements. Combining the finite element (input source) with a surrogate model (data-driven approximation) yields substantial settlement outcomes for structure evaluations. A case study is then used to validate the effectiveness and applicability of this framework. Finally, an exhaustive search approach is used to design a cost-effective improved ground within ultimate and serviceability limit state constraints. Pareto front is computed using a logistic function at different settlement reliability levels.

1. Introduction

For soft clays, uncertainties in material properties (such as hydraulic conductivity, creep index, and constitutive parameters) potentially impact the time-dependent performance of geostructures constructed over them (Karstunen et al., 2015; Karstunen and Yin, 2010). Uncertainty is an intrinsic feature of soils (Mašín, 2015) due to various factors such as measurement scatter arising from the limitations of experimental techniques, inherent spatial variability of soil properties and statistical uncertainty due to limited sampling. The uncertainty can be mainly divided into two categories: the local uncertainty at a specific location and spatial uncertainty across multiple locations. The correlations derived from simple algebraic, statistical approaches, or machine learning-based methods, generally ignore the uncertainty induced by insufficient samples and measurement scatter, producing deterministic predictions without assessing intrinsic uncertainty. Epistemic uncertainty is a type of uncertainty associated with insufficient knowledge of the modeling process (Kendall and Gal, 2017). Hereafter, uncertainty refers specifically to the epistemic and local uncertainty unless otherwise stated.

Basal reinforced piled embankments (BRPEs) are an effective solution to maintain the stability of embankments over thick soft clay deposits (Nguyen et al., 2023; Wang et al., 2023). They help enhance the bearing capacity and subsoil shear strength (Liu et al., 2023), while controlling compressibility and long-term settlement (Dang et al., 2021; Nguyen et al., 2023). Commonly used vertical reinforcing elements include deep mixing columns (Jamsawang et al., 2016; Liu and Rowe, 2015), stone columns (Zhang et al., 2021c; Zheng et al., 2020), cement

* Corresponding authors at: 2 Daliushu Rd, Haidian District, Beijing 100081, China (T. Li). School of Civil Engineering, Southwest Jiaotong Univ, Chengdu 610031, China (Q. Luo).
E-mail addresses: w@swjtu.edu.cn (T. Wang), 230228909@seu.edu.cn (W. Chen), typhoon_li@163.com (T. Li), D.Connolly@leeds.ac.uk (D.P. Connolly), lqrock@swjtu.edu.cn (Q. Luo), kaiwen.liu@queensu.ca (K. Liu), zwsheng@hit.edu.cn (W. Zhang).

https://doi.org/10.1016/j.compgeo.2023.105498
Received 7 November 2022; Received in revised form 30 March 2023; Accepted 22 April 2023
Available online 4 May 2023

fly-ash gravel (CFG) (Yoobanpot et al., 2020; Zhang et al., 2018), and prefabricated high-strength concrete (PHC) piles (Wu et al., 2019a). Basal reinforcement usually refers to the geosynthetic-reinforced (Alkhorshid et al., 2021; Ling et al., 2021; Nguyen et al., 2022), lime/-cement stabilized, or fiber-reinforced load transfer platform (granular cushion) (Dang et al., 2021; Okyay and Dias, 2010) located at the base of an embankment. It has been recognized that the post-construction settlement impacts the serviceability of BRPEs and their structural design optimization, particularly in soft ground conditions (Liu and Rowe, 2015; Zhou et al., 2016). Predicting the time-dependent performance of BRPEs in the presence of uncertainties in subsoil properties can be challenging (Guo et al., 2023; Pham et al., 2022; Phutthananon et al., 2021).

A theoretical framework (Gal and Ghahramani, 2016) that combines neural networks and Monte Carlo dropout for Bayesian appropriation has recently been proposed to study the impact of uncertainty on soil behavior. This technique, abbreviated NN-MCD, correlates soil properties with available experimental data that exhibits intrinsic uncertainty (Zhang et al., 2021a). It has been shown to exhibit predictive performance when a complete set of data is not available for the specification of the soil model. Numerical simulations are an affordable alternative to field testing and scaled physical models to conduct deterministic analysis of embankment settlements. However, it requires high computational cost when employed to analyze all possible combinations of input parameters for problems such as BRPEs. Surrogate modeling (aka emulator or metamodel) is an alternative approach (He et al., 2021) to numerical modelling, that can minimize the computational burden by constructing an approximate model for the long-term performance evaluation of BRPEs. Combining a surrogate approach with NN-MCD can potentially provide a solution to the above-mentioned challenges with estimating embankment settlements. Similarly, it can allow for the structural optimization of BRPEs with respect to settlement, while incorporating uncertainty.

In this study, first, a hybrid modeling approach for embankment settlements is described. It contains three sections: uncertainty modeling of subsoil mechanical properties, deterministic hydromechanical FE analysis of reinforced embankments on soft clay, and surrogate-assisted probabilistic analysis of post-construction settlements. The applicability of the proposed modelling methodology is demonstrated through a detailed case study. Next, probability distributions of settlements are introduced into the structural optimization of reinforced embankments. Finally, cost − benefit analysis is performed based on the relationship between construction costs and expected settlements at different reliability levels.

2. Modeling framework

To evaluate the influence of uncertainty on the time-dependent behavior of reinforced embankment systems, post-construction settlement calculations should be capable of incorporating uncertainty due to the variance of natural soil properties. To do so, this paper proposes a data-driven modeling framework to meet this objective. The framework is described in a general way as follows:

1) Generate random soil properties from a known experimental database. Identify fundamental soil properties (e.g. constitutive model parameters) that exhibit inherent variability and control the long-term performance of geo-structures. Correlate the soil properties with common index properties (e.g. plasticity index) while accounting for epistemic uncertainty.
2) Perform deterministic analysis using numerical simulations (e.g., FEM). A few representative simulation cases (sample selection) are selected and calculated to compile a dataset of settlements. Each simulation is run with fixed values of soil properties as inputs, but soil properties may vary across different cases. This operation ensures the outcomes of the uncertainty modeling can be related to the deterministic analysis.
3) Develop a surrogate model for the purpose of minimizing the computational effort required to execute a large number of simulation evaluations needed for risk analysis. The surrogate model is constructed using a data-driven, bottom-up approach to obtain input − output behavior.
4) Combine the deterministic analysis with the surrogate model to conduct probabilistic analysis of the index of interest.

2.1. Uncertainty modeling using NN-MCD

This section proposes an uncertainty modeling approach for projecting soil properties from an experimental database of relevant and easily accessible index properties based on prior knowledge. Neural network (NN) is a widely accepted tool for possible correlations. In the conventional NN framework, the values of its weight and bias and the model architecture are deterministic (Zhang et al., 2021b). A Bayesian neural network (BNN) has been devised to combine the predictive power of machine learning algorithms with uncertainty. By incorporating a Bayesian approach into the traditional NN method, the parameters' uncertainties can be quantified. This integration enables the training of a BNN, akin to conventional Bayesian learning, to obtain the posterior distribution of the weights and biases, which are treated as a multivariable distribution, rather than scalar values. However, BNN models are computationally expensive. Alternatively, to account for the uncertainty effect, Monte Carlo dropout (MCD) for Bayesian approximation is incorporated into the neural network to develop a neural network with Monte Carlo dropout (NN-MCD). This approximation has been shown to have a reasonable performance (Zhang et al., 2022). Consequently, the connections between neurons will be randomly deleted at a predefined probability, and model uncertainty is achieved by modifying the architecture (Fig. 1). MCD's lower computational cost and explicit framework make it an effective tool for recognition tasks, while also reducing the likelihood of overfitting in neural networks. The dropout operation is activated during both the model training and testing phases; the necessary modules thus are compatible with those in the activation function and optimizer of the general neural networks. Its architecture is flexible because the probability of each connection being inactivated is fixed during implementation (Gal and Ghahramani, 2016). The standard output and uncertainty after performing T stochastic calculations through the network are expressed as:

$$\mathrm{E}(\boldsymbol{y}) = \frac{1}{T}\sum_{i=1}^{T}\boldsymbol{y}_i(\boldsymbol{x}, \boldsymbol{W}_i, \boldsymbol{b}_i)\# \tag{1a}$$

$$Var(\boldsymbol{y}) = \frac{1}{T}\sum_{i=1}^{T}\left[\boldsymbol{y}_i(\boldsymbol{x}, \boldsymbol{W}_i, \boldsymbol{b}_i)^T\boldsymbol{y}_i(\boldsymbol{x}, \boldsymbol{W}_i, \boldsymbol{b}_i) - \mathrm{E}(\boldsymbol{y})^T\mathrm{E}(\boldsymbol{y})\right] \tag{1b}$$

where $\times$ and $\boldsymbol{y}$ are the input and output, respectively; $\boldsymbol{W}_i$, $\boldsymbol{b}_i$, and $\boldsymbol{y}_i$ are

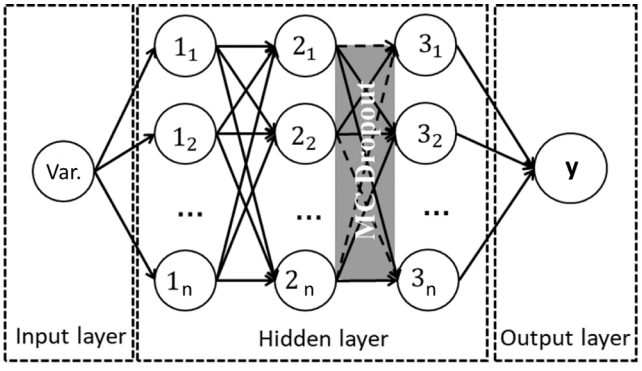

Fig. 1. Architecture of a neural network with Monte Carlo (MC) dropout.

the weight, bias, and output at the i^{th} calculation.

The grid search method (Chen et al., 2022) is used to determine the optimal number of neurons and hidden layers. A mean squared error (MSE) function with k-fold cross-validation is employed as the loss function, formulated as:

$$L(\boldsymbol{y}^a, \boldsymbol{y}^p) = \frac{1}{k}\sum_j \frac{1}{m}\sum_i \left(\boldsymbol{y}_i^a - \boldsymbol{y}_i^p\right)^2 \tag{2}$$

where $\boldsymbol{y}^p$ and $\boldsymbol{y}^a$ denote the predicted and actual outputs; $k = 10$, corresponding to 0.1 for the validation split ratio of the training set; m is the number of training samples within k-fold. The rectified linear unit (*ReLU*) is used as the activation function to minimize the probability of saturation challenges. It is expressed as:

$$ReLU(x) = \begin{cases} x, x > 0 \\ 0, x \le 0 \end{cases} \tag{3}$$

A gradient descent optimization algorithm automatically updates the weights and biases of the NN-MCD. The number of training datasets for each epoch is selected according to the batch size, and sufficient training epochs are used to achieve convergence of the loss values. The general framework for the NN-MCD approach is developed by determining some necessary presets (hyperparameters).

2.2. Surrogate modeling using BPNN

Currently, there exist two common methods to simulate the variability of foundation soil parameters: the single random variable (SRV) approach and the random field (RF) approach. The SRV approach treats each layer of foundation soil as a homogeneous media and employs varying probability distributions to describe the variability of soil properties. However, this method is limited in its ability to consider the variations in soil mechanical properties across spatial locations. In contrast, the RF approach outperforms the SRV approach by capturing this spatial variability. Both approaches typically require a large number of calculations using Monte Carlo simulations to obtain the desired distribution.

Exploring all combinations of variables for probabilistic analysis using FE simulations is challenging due to high computational cost. Surrogate models are used to reduce computational effort by mapping nonlinear relationships between input and output variables, based upon a limited number of training samples, computed for example using FE techniques (He et al., 2022). They can then capture input − output behaviors for scenarios where FE simulations have not been previously computed (He et al., 2020). In the case of RF, the number of inputs to the surrogate model often exceeds several hundred, making it less competitive in some scenarios. Settlement distributions calculated by SRV and RF generally agree well when the variability of soil properties is only along the depth, and the distance correlation is large. However, when the distance correlation is small, the means of the distributions generated by SRV and RF are comparable, but the standard deviation of the SRV-derived distributions is larger than that of its RF-derived counterpart (Alibeikloo et al., 2022). This study uses the upper 95% quantile of the settlement distribution for subsequent design to ensure computational efficiency and conservative design solutions.

A backpropagation neural network (BPNN) algorithm is used to train feedforward neural networks, computing gradient weights via a loss function (Rumelhart et al., 1986). The predictive performance of BPNN depends on the number of hidden neurons and hidden layers. If the general architecture is defined, the weights and bias can be obtained using gradient descent. To further improve the generalization ability of BPNN for case-specific applications, it's architecture can include predefined groups of predictor variables that maintain model accuracy while avoiding redundant calculations. As an illustration in Fig. 2, eight example parameters are divided into two subgroups: structural related parameters and soil strength related properties. Then, variables within the same group will have similar effects on outputs, whereas variables from different groups can have a diversified impact on outputs with limited interaction. If subgroups are established for inputs, the connections between input and hidden neurons will not be mixed until reaching the next hidden layer. In this case, two hidden layers are used for structural and soil parameters, which can be adjusted for case-specific applications.

Given a set of input values $\times$, the mathematical description of the established model is expressed as:

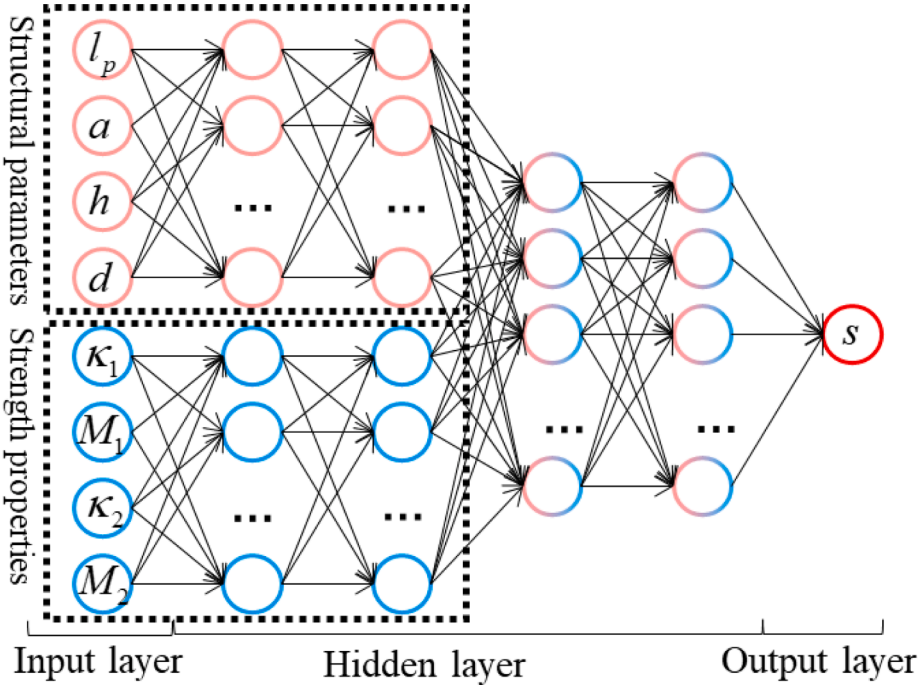

Fig. 2. Schematic of the internally devised BPNN architecture.

$$\boldsymbol{H}_1 = ReLU(\boldsymbol{W}_1 x + \boldsymbol{b}_1) \tag{4a}$$

$$\boldsymbol{H}_2 = ReLU(\boldsymbol{W}_2 x + \boldsymbol{b}_2) \tag{4b}$$

$$\boldsymbol{H}_3 = ReLU(\boldsymbol{W}_3 x + \boldsymbol{b}_3) \tag{4c}$$

$$y = \boldsymbol{W}_4 \boldsymbol{H}_3 + b_4 \tag{4d}$$

where $\boldsymbol{H}_1$, $\boldsymbol{H}_2$, $\boldsymbol{H}_3$, and y are the outputs of first, second, third hidden layers and the final output layers, respectively. $\boldsymbol{W}_1$, $\boldsymbol{W}_2$, $\boldsymbol{W}_3$, and $\boldsymbol{W}_4$ are the weight matrices, while $\boldsymbol{b}_1$, $\boldsymbol{b}_2$, $\boldsymbol{b}_3$, and b_4 are the bias vectors.

2.3. Evaluation metrics

The following three metrics are applied to evaluate the performance of the proposed NN-MCD and BPNN models: the coefficient of determination R^2, root mean square error (RMSE), and mean absolute percentage error (MAPE).

$$R^2 = 1 - \frac{\sum_{i=1}^{n} (y_i^p - y_i^a)^2}{\sum_{i=1}^{n} (y_i^a - \overline{y}_i^a)^2} \tag{5a}$$

$$RMSE = \sqrt{\frac{1}{n}\sum_{i=1}^{n} (y_i^p - y_i^a)^2} \tag{5b}$$

$$MAPE = \frac{1}{n}\sum_{i=1}^{n} \left| \frac{y_i^p - y_i^a}{y_i^a} \right| \times 100\% \tag{5c}$$

where n denotes the total number of datasets; $\overline{y}_i^a$ is the mean of the observed results; n is the sample size. The metrics are measured separately for the predicted soil parameters and post-construction settlement.

2.4. Probabilistic analysis of settlements

Fig. 3 shows the flowchart for the proposed probabilistic analysis of post-construction settlements of basal reinforced piled embankments overlying multilayered soft soils. In this illustrative example, DM columns are inserted as vertical reinforcement and a fiber-reinforced load transfer platform (FRLTP) is used as horizontal reinforcement. The case-specific process is:

1. Identify the fundamental structural parameters (e.g. pile length and spacing) as design variables and their corresponding design space based on site conditions, construction techniques, and design requirements;
2. Assess the uncertainty in soil properties (e.g. strength parameters from soil constitutive models) and perform predictions by validated NN-MCD algorithm, yielding a collection of input vectors (M_1, M_2, κ_1, κ_2);
3. A numerical model is developed for basal reinforced piled embankment and is verified against field case history. A set of representative design scenarios are selected using the orthogonal design method and their post-construction settlements are computed using deterministic numerical simulations;
4. Simulations that produced excessive deformation (convergence difficulties) are rejected while the remaining datasets become the sample database. These are divided into training and test sets that are used for developing a surrogate model (BPNN with two individual input layers).
5. For each possible combination of design variables, the probability distribution of post-construction settlements is calculated using the surrogate model.

In summary, the structural parameters are fed into the BPNN model for structural optimization while the soil (strength) properties are fed in for uncertainty impact. The proposed probabilistic analysis framework can be extended to more complex geotechnical structure problems.

3. Case study

The implementation of the proposed methodology is demonstrated through a case study. Each section of the modeling framework is validated separately. The finite element method is employed to obtain the deterministic post-construction settlements of basal reinforced piled embankments (Ma et al., 2021). Further, the hydromechanical model is

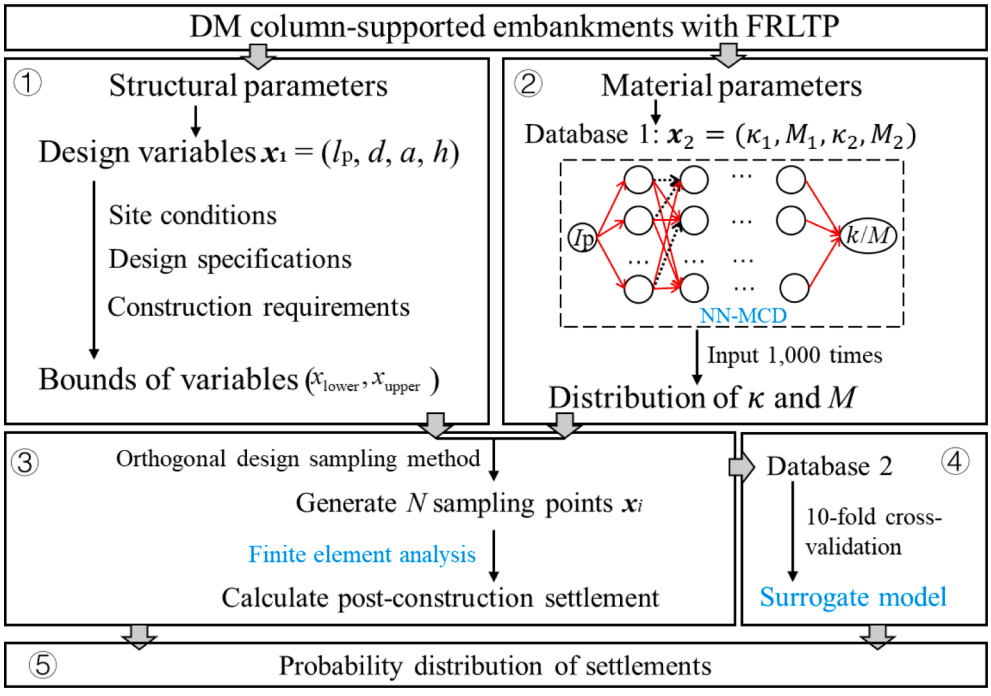

Fig. 3. Flowchart for the settlement probability analysis of basal reinforced piled embankments over soft ground.

developed based on a well-documented field test history (Chai et al., 2017, 2015; Dang et al., 2021). The model construction process and site conditions are briefly introduced, emphasizing the modifications made to uncertainty modeling of soil parameters.

3.1. FE model

A FE model was developed of a 6-m-high embankment overlying a multilayered soft soil, supported by DM columns and a reinforced cushion (Vivi et al., 2015). The geometry and meshing of the support system is shown in Fig. 4, only right half of the domain is shown due to symmetry. The embankment was constructed on a 1-m-thick surface layer, underlain by an 11-m-thick deposit of soft clay, divided into upper and lower portions due to the difference in their mechanical properties. Below the soft soil is a 3-m-thick stiff clay layer and 15-m-thick sand stratum. The properties of each soil layer and embankment fill are provided in Table 1. A 0.5-m-thick fiber-lime-treated granular layer (Vivi et al., 2015) is adopted for the load transfer platform over pile tops. The floating DM columns have a diameter of 1.2 m and a total length of 10 m, leaving 2 m of unreinforced soft soil below the pile toes. The unconfined compressive strength, tensile strength, and undrained shear strength of the DM columns are prescribed as 1000 kPa, 150 kPa, and 500 kPa, respectively (Dang et al., 2021). The construction sequence was simulated by compacting the fills in lifts of 0.5 m at 0.06 m/d. Suppose a termination criterion of 0.1 mm/a for the settlement rate (Chen et al., 2021); in that case, the consolidation period could be prescribed as 15 years to approximate the final post-construction settlements. Secondary consolidation, also known as creep, is not included in this analysis.

A two-dimensional plane strain model was established using the commercial software PLAXIS 2D based on a conversion approach (Chai et al., 2015; Vivi et al., 2015; Zhang et al., 2019; Dang et al., 2021). The DM columns are modelled as 0.6-m-wide continuous plane-strain walls that result in an area replacement ratio of 31%, accounting for the equivalent axial stiffness (EA). The center-to-center wall spacing is 1.9 m, the same as the center-to-center column spacing. A Mohr – Coulomb (MC) model is used for the linear elastic–perfectly plastic properties of DM columns (Liu and Rowe, 2015; Zhang et al., 2019), fills, cushion, and sand. The mechanical performance of both the soft soil layers and surface soil layer is represented using the Modified Cam Clay (MCC) model. The variation of hydraulic conductivity (k) due to the embankment loading is expressed as a function of the void ratio (e) (Taylor, 1948):

$$\log k = \log k_0 - \frac{2(e_0 - e)}{e_0} \tag{6}$$

where k_0 and e_0 are the initial hydraulic conductivity and void ratio, respectively. An impermeable boundary is applied to the right and left sides of the model (Zhang et al., 2019), while pore fluid flow is allowed at the model's ground surface and bottom. Roller supports are used for both sides, and a pinned boundary is employed at the bottom. Drained behavior is considered for the embankment fill and sand layer, while the other system elements behave in an undrained condition. (15)-node triangular elements are used for all the meshes, with extra excess pore water pressure considerations for the DM columns and reinforced cushion. The shear behavior at the cushion – soil and column – soil interfaces is modeled by introducing the shear strength reduction factor, $R_{int} = 0.8$ in this case (Wu et al., 2019b; Yapage and Liyanapathirana, 2014). Fig. 5 compares predicted settlement at points B and C against field observations of the same locations (Dang et al., 2021). It is demonstrated that the proposed numerical approach is reasonable.

3.2. Uncertainty in constitutive soil parameters

3.2.1. Data source

If embankments are to be constructed on soft ground, the mechanical behaviors of soft deposits can be a concern. The Modified Cam-Clay (MCC) model is a well-established constitutive model to describe the strength, compression, and critical state of the soft subsoils. Although κ and M of the MCC model have been provided in Table 1 based on laboratory tests, the proposed NN-MCD approach generates random values for κ and M, which are associated with the plasticity index. The NN-MCD algorithm is applied for the uncertainty modeling of three MCC constitutive parameters: critical state ratio M, isotropic swelling index κ, and logarithmic hardening modulus λ. The consolidation settlement of soft ground is significantly influenced by the λ parameter, which is closely related to κ. On the other hand, the plastic deformation of soft subsoil is highly affected by the M parameter. This is because subsoil can easily reach a plastic state when the M value is low. Therefore, to account for uncertainty, these three constitutive parameters have been selected as inputs. Fifty parallel simulations were performed for the same design scenario; the input parameters κ, M, λ=10κ for each layer of soft clay were assigned different values based on Monte Carlo simulations (MCS) during each run. In practice, κ is usually chosen in the range: $\lambda/10$ - $\lambda/3$. Consequently, if the uncertainty of κ and M is considered in the

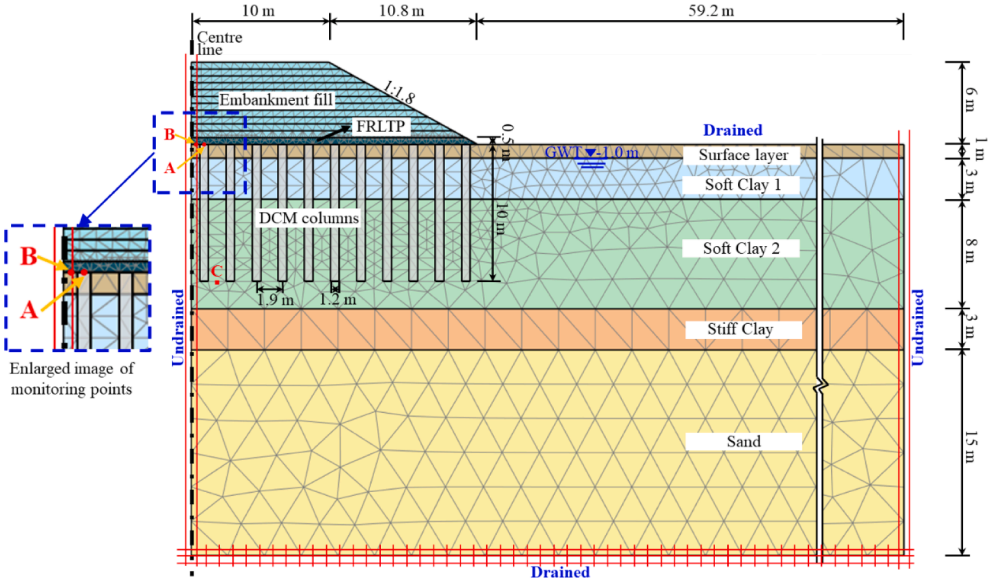

Fig. 4. Meshing and boundary conditions of the 2D basal reinforced piled embankment model: Points A, B, and C indicate the monitoring locations.

Table 1
Material models and associated parameters in FE modeling (Chai et al., 2015; Dang et al., 2021; Vivi et al., 2015).

Material	Model	E (MPa)	υ	C′ (kPa)	$\varphi(^\circ)$	λ	κ	M	e_0	$k_v(10^{-4}$ m/day)	$k_h(10^{-4}$ m/day)	OCR
Surface layer	MCC	—	0.15	—	—	0.25	0.025	1.2	1.5	6	9.1	1.5
Soft clay 1	MCC	—	0.15	—	—	0.87	0.087	1.2	3.1	4.4	6.6	2.5
Soft clay 2	MCC	—	0.15	—	—	0.43	0.043	1.2	2.5	4.6	6.9	1.2
Stiff clay	MCC	—	0.15	—	—	0.12	0.012	1.2	0.8	25	25	1.0
Sand	MC	20.0	0.10	20.0	35.0	—	—	—	0.7	250	250	—
FRLTP	MC	125.8	0.32	75.0	42.0	—	—	—	—	—	—	—
Fill	MC	1.0	0.40	20.0	35.0	—	—	—	—	—	—	—
DM columns	MC	100.0	0.15	500.0	—	—	—	—	—	4.6	4.6	—

Note: $c^{'}$, effective cohesion; OCR, over-consolidation ratio.

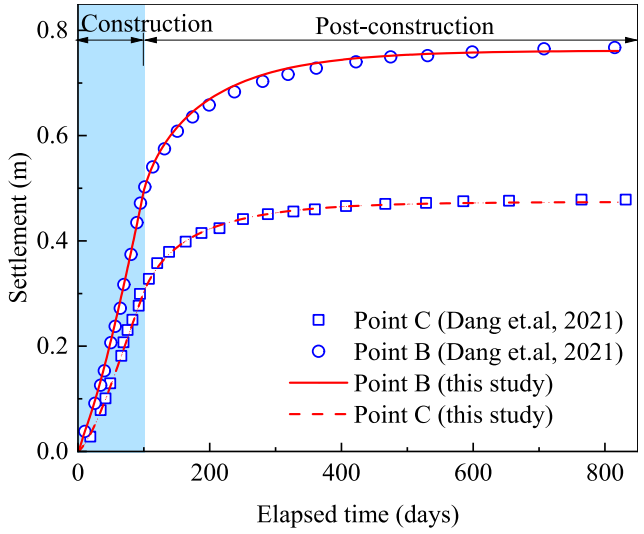

Fig. 5. Time histories of numerical settlement predictions at Points B and C compared against the field measurements (Dang et al., 2021).

reliability analysis of post-construction embankment settlements, λ can be sequentially determined based on the value of κ.

It was reported in (Zhang et al., 2021a) that it is possible to predict the creep index and hydraulic conductivity of soft clays using three soil index properties. Previous investigations have also shown that the parameters for a MCC model can be approximated by the Atterberg limits (Akio et al., 1988; Burland, 1990; Yoon et al., 2004). Linear correlations between the Atterberg limit and the soil parameters for constitutive relations were experimentally found to have high correlation coefficients (Akio et al., 1988). The database for training the ML-based model was formed by collecting a total of 69 datasets of κ and 24 datasets of M (Akio et al., 1988) with the same single influential variable, Atterberg limit (I_p). Table 2 shows the statistical properties of the database. The experimental datasets are randomly divided into 20% and 80% portions for testing and training purposes. Note that min–max normalization is employed for feature scaling so each feature contributes (approximately) proportionately to the final output.

3.2.2. Model construction

A suitable architecture for the NN-MCD model was developed to have optimal weights and biases. This section presents an architecture comparison and hyperparameter selection with scientific methods for model development. The number of hidden layers and neurons are two fundamental factors describing the model architecture. The number of hidden layers in the trial architectures was increased from 1 to 4 in increments of 1, and the number of hidden neurons within a range of 10 and 100, in increments of 10, giving a total of 400 trials (10 trials for each architecture). Although the desirable weights and biases can be determined after these training, the dropout-induced random model connection can produce various outputs per calculation in the same set of input parameters conditions. The final prediction must be the mean of 80 stochastic calculations (Eq. 1).

Fig. 6 demonstrates a comparison of R^2 values of NN-MCD on training and test sets considering the number of hidden layers and neurons. Other configurations are kept the same, including the total number of epochs = 8,000 and batch size = 3. The predictive performance of NN-MCD typically improves with increased hidden layers and neurons, as a complex architecture enhances the model's mapping capability. The prediction of M and κ exhibits a similar trend, and an identical architecture is identified for these two parameters. The grid search method has been used to determine the optimal combination of architecture parameters, find a simpler model architecture, and hence reduce the computational cost. Three hidden layers and 50 neurons are employed to develop the NN-MCD-based model for predicting M and κ.

Dropout probability also has a fundamental influence on architecture. In the implementation, an NN-MCD-based model is trained ten times with a variation of initial biases and weights. The optimal dropout probability is then selected after comparing and evaluating the predictive performance between all dropout probabilities concerned (ranging from 0.1 to 0.5). The mean of 80 stochastic calculations performed for each group of input parameters is obtained for the final output. Fig. 7 illustrates the dropout probability impact on the NN-MCD model for M and κ, respectively, while the boxplot shows the range of calculated R^2. With the increase in dropout probability, a simpler architecture and poorer mapping ability are anticipated with more connections cut, and larger variations have been observed on the training set with much lower R^2. The R^2 in the test sets exhibits a similar trend for κ. However, the values of R^2 vary significantly with the dropout probability for M. The optimal dropout probability is 0.1 because the predictive performance on both training and test sets is relatively consistent, yielding the largest R^2.

In this case, the weight matrices $\boldsymbol{W}_1$, $\boldsymbol{W}_2$, $\boldsymbol{W}_3$, and $\boldsymbol{W}_4$ (Eq. 4) have sizes of 50 × 1, 50 × 50, 50 × 50, and 1 × 50, respectively. The bias vectors $\boldsymbol{b}_1$, $\boldsymbol{b}_2$, $\boldsymbol{b}_3$, and $\boldsymbol{b}_4$ (Eq. 4) have sizes of 50 × 1, 50 × 1, 50 × 1, and 1 × 1, respectively. A total of 5,251 weights and biases were automatically optimized during the model training process.

Table 2
Statistical measurements of the experimental datasets for the NN-MCD model.

Variable	Sample Size	Min.	Max.	Mean	Std. Dev.
$\kappa(\times 10^{-2})$	69	0.41	17.60	4.20	3.32
M	24	1.27	1.69	1.61	0.10
I_p	93	4.09	65.44	30.68	14.45

3.2.3. Predictions

The optimal configuration of the NN-MCD model, including the general architecture, drop probability, activation and loss functions, optimizer, validation split, batch size, number of epochs, and stochastic

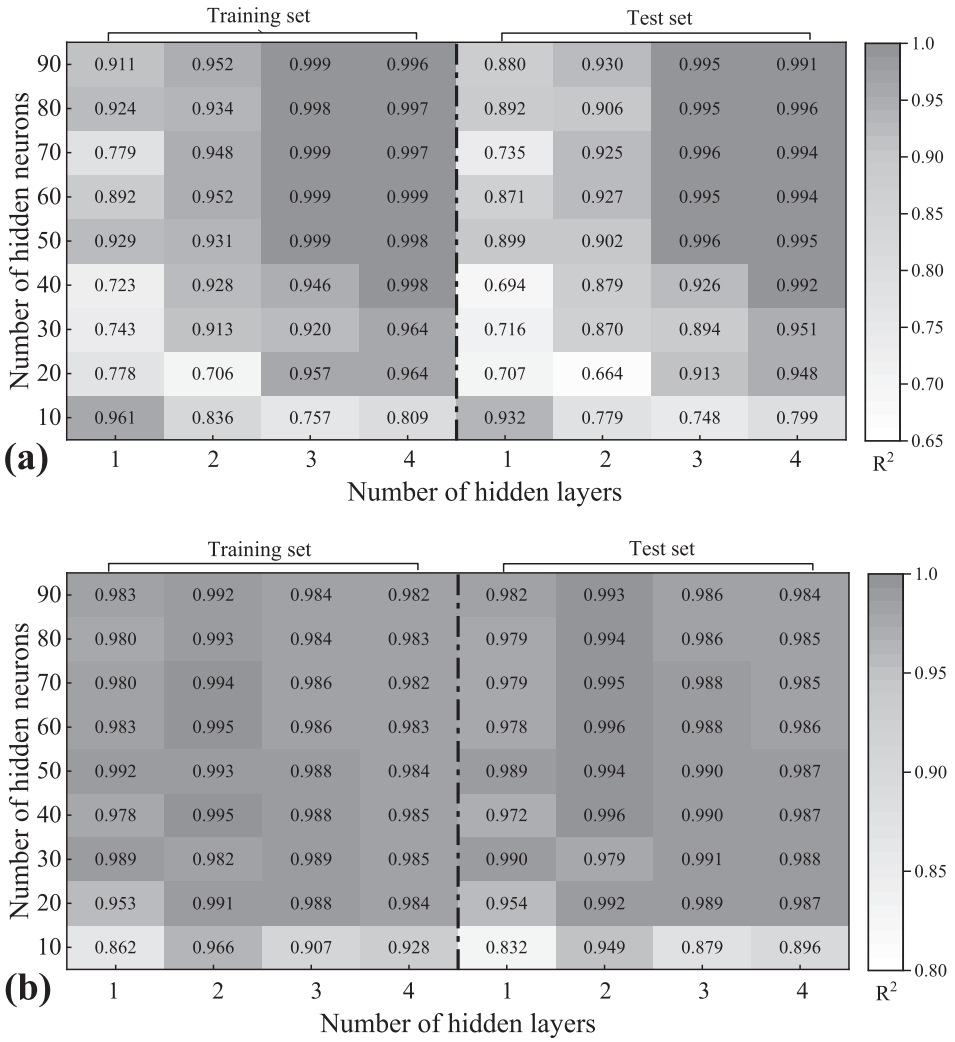

Fig. 6. The R^2 values of NN-MCD with different architectures on training and test sets: (a) parameter M; (b) parameter..κ

calculations, are determined based on the steps mentioned earlier. It has been demonstrated that 8,000 epochs enable the convergence of the training process.

Fig. 8 presents the comparison of experimental and predicted data for two soil parameters (κ and M). Combining these indicators allows for a comprehensive evaluation of model performance (Wang et al., 2021). Most data points in the testing and training sets are located close to the identity line. The prediction errors of M yield $RMSE = 0.008$ and 0.114 in the training and test sets, respectively. Some outliers have been observed in training set for larger values of κ, but κ in the lower range shows better agreement with the experimental results. The comparison in Fig. 8 confirms strong predictive performance of the NN-MCD model for κ and M.

The predicted κ and M with 68%, 95%, and 99.7% confidence intervals are further plotted against the plasticity index in Fig. 9 to reflect the uncertainty of the NN-MCD algorithm. Although more outliers have been found for κ in the higher range, consistent with Fig. 8, most data points are scattered around the 99.7% confidence interval. The correlation between the plasticity index and M is negative, while it becomes positive for the plasticity index and κ, which is consistent with the laboratory observations (Akio et al., 1988). The confidence interval is generally wider for limited data sets, however, narrows for comprehensive datasets because the accuracy of data-driven models is dependent on the sample size. The variations in confidence intervals are contrasting, when comparing κ and M. Although the training data is discrete, the developed NN-MCD-based model can perform continuous predictions across a wide range of plasticity index and capture different trends in κ and M with uncertainty considerations.

Fig. 10 represents the generated data points by NN-MCD for κ and M in the form of frequency distribution with, $I_p = 57$, 30. Note that these two levels of plasticity are selected because they are of interest in the following finite element simulations. One thousand stochastic calculations were conducted on each case based on a Monte Carlo approach. The Kolmogorov–Smirnov test demonstrates that the output of NN-MCD follows a normal distribution curve. The mean and standard deviation correspond to the results at $I_p = 57$, 30 in Fig. 9. Considering only one predictor (I_p) is used in this NN-MCD model, the model performance can be expected to have reduced accuracy compared to reported results (Zhang et al., 2021a) computed using three predictors. Overall, the proposed NN-MCD is suitable to serve as the foundation of the subsequent reliability analysis of settlement.

3.3. Probability analysis of settlements

3.3.1. Development of surrogate model

Fig. 10 shows the uncertainty in the MCC model parameters considering two soft clay layers sandwiched between the surface and stiffened clay (Table 1). λ is calculated as a function of κ, meaning there

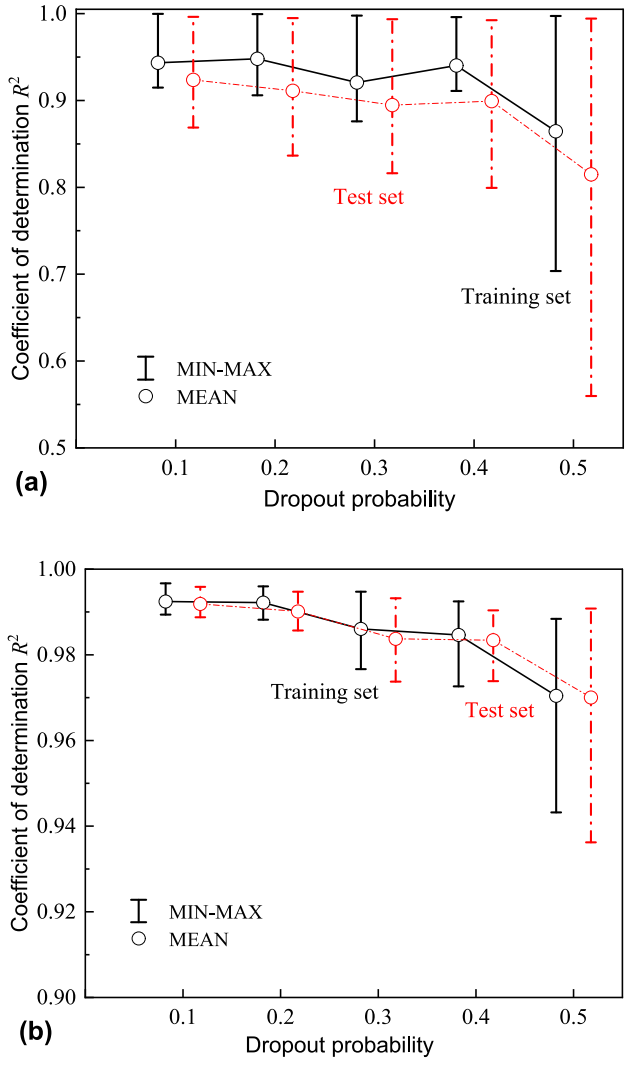

Fig. 7. Dropout probability impact on the predictive performance of the NN-MCD model: (a) parameter *M*; (b) parameter..κ

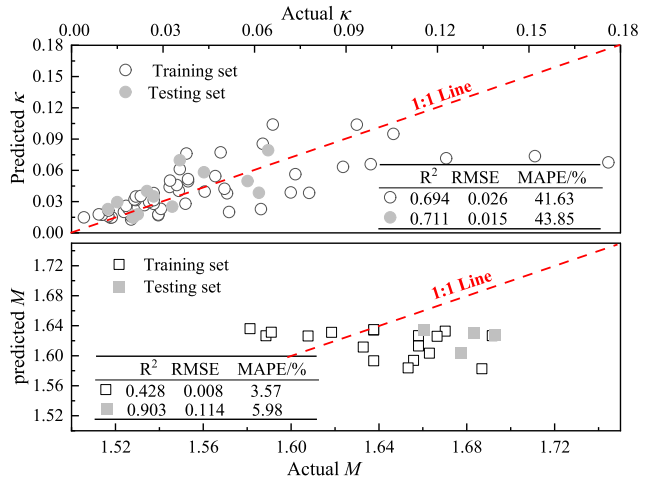

Fig. 8. Comparison of experimental and predicted data: (a) parameter κ; (b) parameter *M*.

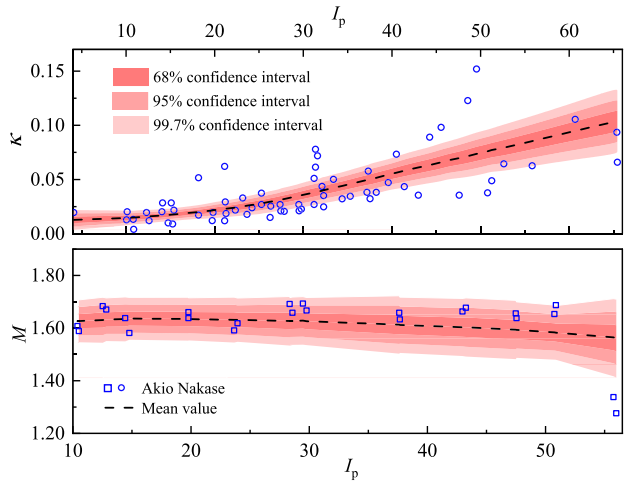

Fig. 9. Evolution of predicted values based on NN-MCD and experimental data along with the plasticity index: (a) parameter *M*; (b) parameter..κ

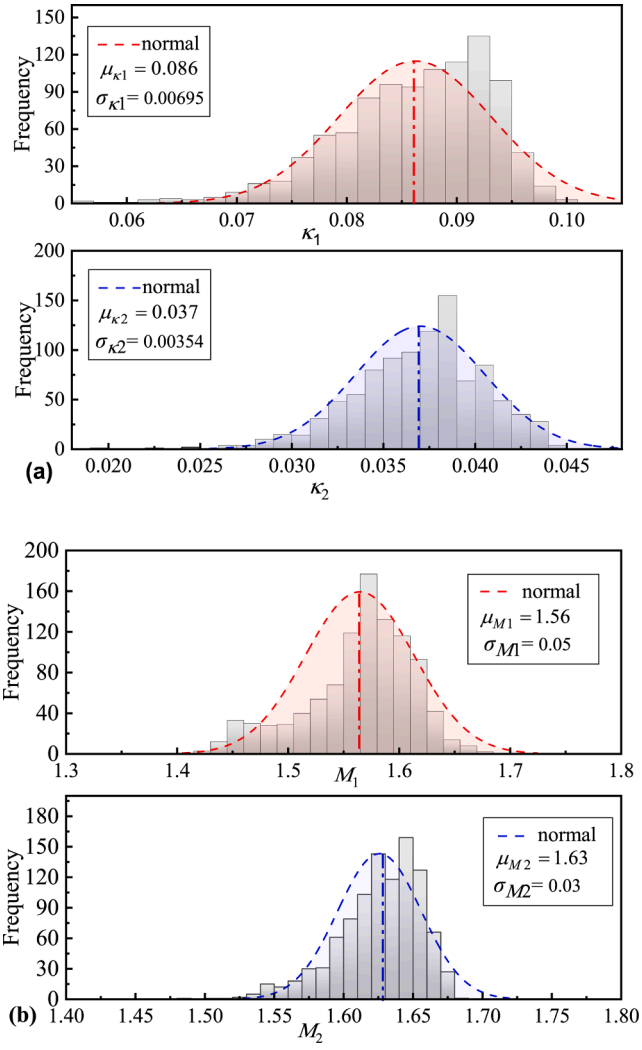

Fig. 10. NN-MCD derived frequency distribution of κ (a) and *M* (b) given I_p = 57 (upper soil layer) and 30 (lower soil layer).

is four independent input variables, κ_1 and M_1 for the upper layer, and κ_2 and M_2 for the underlying layer. This selection is reasonable because the settlement of piled embankments is primarily governed by the

properties of layered soils in field conditions. Note that the other material parameters of interest are deterministic constants (Table 1). In addition to the soil parameters, four structural parameters (design variables), including pile length l_p, pile diameter d, pile spacing a, and thickness of reinforced cushion h, are used for the model geometry. The statistical properties of eight inputs (as part of the initial conditions for the numerical modeling) are provided in Table 3. Note the uncertainty of the soil parameters is quantified using the NN-MCD algorithm for a given I_p (the interval is 1.0 m for l_p and 0.1 m for geometries d, a, and h). The total number of simulation cases is then: $7(l_p) \times 8(d) \times 10(a) \times 8(h) \times 1000(M_1, M_2, \kappa_1, \kappa_2) = 4.48 \times 10^6$.

To shortlist the simulations to be computed, initial sample selection was performed using an orthogonal design before constructing a surrogate model. Through the optimization of the dataset size, 243 cases were selected as representative samples. It is known from the numerical simulations that 98 out of 243 cases failed to converge due to excessive deformation, so they were removed from the dataset used to develop the surrogate model. 20% of 145 valid cases were randomly chosen to structure a test set, and the remaining 80% were used for the training set.

The sample points are first normalized to the (0, 1) range using the min–max normalization method that guarantees all features have the same scale, expressed by

$$x_{norm} = \frac{x - x_{min}}{x_{max} - x_{min}} \tag{7}$$

where x_{norm} is the normalized value, x is the original data point, x_{max} and x_{min} are the maximum and minimum values. The training of the BPNN-based model involves the determination of optimal architecture and hyper-parameters, which have been extensively discussed (Zhang et al., 2021b; Zhang et al., 2021d).

3.3.2. Performance evaluation

Fig. 11 shows the scatter plots of predicted post-construction settlement using the surrogate model to derive FEM computed outputs, considering training and test sets, along with statistical performance indicators. The BPNN-derived settlements match the numerical results well, and the predictive performance in both training and test sets is consistent, exhibiting similar performance indicator values. All indicators confirm the generalization ability of the BPNN-based model, and this model is thus incorporated into the probabilistic design framework as a suitable surrogate modeling approach. BPNN effectively balances the requirements of intelligibility and predictive accuracy, especially for test data acquired from numerical simulations with high signal-to-noise ratios. The optimal configuration of the BPNN model is two hidden layers, each with 32 hidden neurons, ReLU as the activation function, Adam (adaptive moment estimation) as the optimization algorithm, and a maximum of 100 iterations.

Fig. 12 represents the sensitivity analysis results. The contribution of each input variable to the post-construction settlement is considered reasonable in terms of FEM calculations for a real-life case. In order of importance, four design variables are critical factors for settlement: pile length, pile diameter, pile spacing, and the thickness of the cushion. However, the importance of predictors for the uncertainty in soil properties is marginal, adding up to 7.2% of total contributions. Pile length plays a fundamental role in the development of settlement because it matters most whether the pile toe has reached the layer of stiffened clay or not. The uncertainty in soil properties may influence the post-construction settlement, but this effect is likely to be less profound than that of the design variables in most real-world scenarios.

Table 3
Statistical measurements of the simulation datasets for the surrogate model.

Variable	Min.	Max.	Mean	S.D.
$\kappa_1(\times 10^{-2})$	6.53	10.71	8.77	0.96
M_1	1.37	1.68	1.56	0.05
$\kappa_2(\times 10^{-2})$	2.0.64	4.76	3.77	0.49
M_2	1.49	1.68	1.63	0.03
l_p(m)	6.00	12.00	8.86	1.92
d (m)	0.80	1.50	1.10	0.20
a (m)	1.60	2.50	2.08	0.28
h (m)	0.20	0.90	0.52	0.24

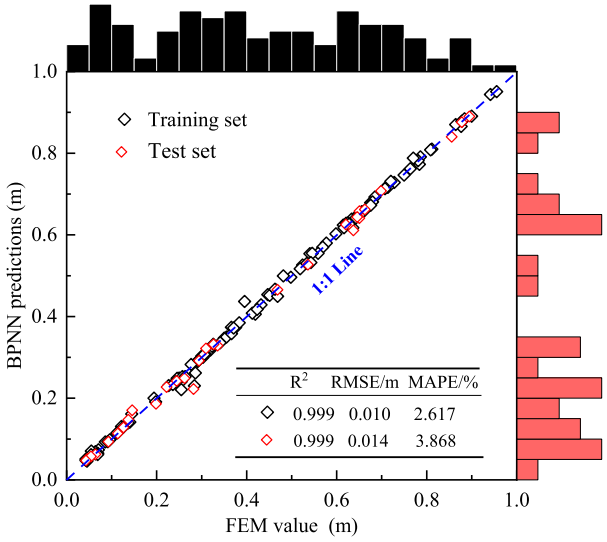

Fig. 11. Predictive performance of the surrogate model compared against FE analyses.

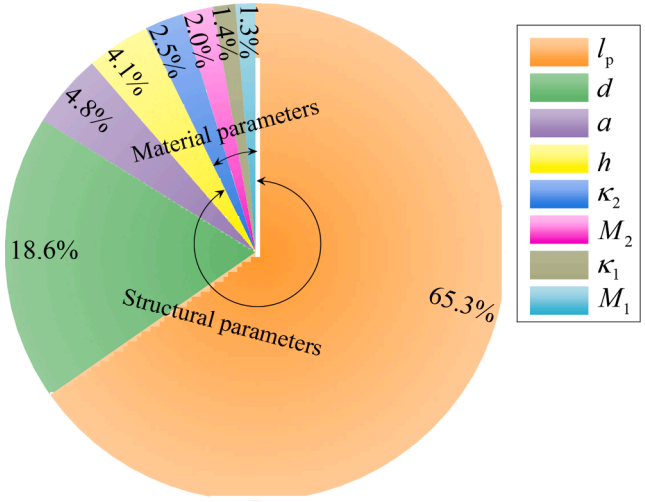

Fig. 12. Feature importance of the RF-based surrogate model concerning post-construction settlement.

3.3.3. Probabilistic distribution of settlements

Given a particular set of design variables, 1,000 input vectors (M_1, M_2, κ_1, κ_2) are first generated from stochastic calculations using the NN-MCD algorithm, then fed into the validated BPNN-based surrogate model, resulting in a total of 1,000 outputs of post-construction settlement. Concerning the simulation case specified in Fig. 4, the frequency of predicted settlements is displayed in Fig. 13. The Kolmogorov-Smirnov test is performed, showing that the set of settlements follow a normal distribution with mean and standard deviation, being 0.23 and 0.021 respectively. It is recommended to use a target reliability index within a range of 1.0 to 2.5 for SLS of railway infrastructures, as per China's design code (MOHURD, 2019); for $RI = 1.96$ (probability of

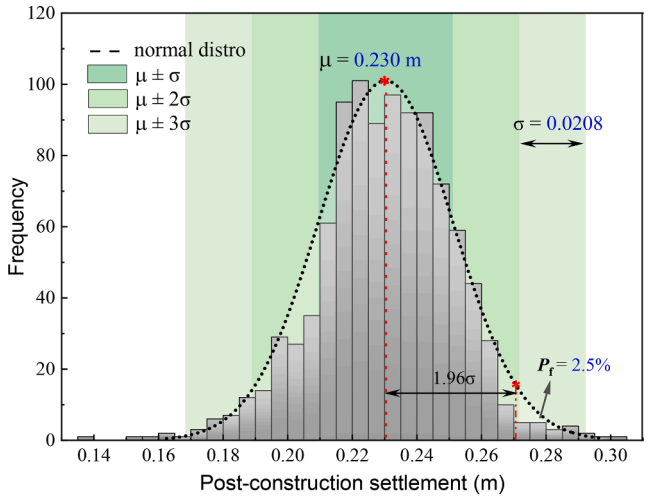

Fig. 13. Probability distribution of surrogate-based post-construction settlement considering uncertainty (simulation conditions specified in Table 2 and Fig. 8).

failure $P_f = 2.5\%$), the corresponding settlement is 0.27 m. This example demonstrates that surrogate modeling for each combination of design variables can efficiently determine the frequency distribution of post-construction settlement.

4. Settlement-based structural optimization

As an illustration of potential application, the calculated probability distribution of post-construction settlements can be used to assist the structural optimization of reinforced embankments. The procedure is performed by establishing a settlement-based optimization problem, which is solved to determine the Pareto fronts when all design constraints and requirements are satisfied.

4.1. Variables and constraints

During the design process, the geometry of the embankment, including the height, crest width, and slope gradient, is generally predefined per the specification requirements and traffic analysis (Yang et al., 2021). The mechanical properties of FRLTP may be fixed values and vary slightly according to regional construction practices. Therefore, the general configuration of embankments and material properties of FRLTP (affected by the addition of fiber reinforcement and soil stabilization techniques) are not treated as design variables in this investigation. The critical design parameters of interest encompass the pile diameter d, pile length l_p, pile spacing s, and the thickness of FRLTP h, in the case of basal reinforced DM column-supported embankments, as shown in Fig. 14.

The design constraints fall into three main categories: site conditions, constructability, and specification requirements. The geotechnical design must recognize feasible FRLTP and DM column-supported embankment designs with a limited range of design variables in design space. The limit state requirements of concern, such as serviceability limit state (SLS) and ultimate limit state (ULS), should also be satisfied. The design results are also dependent upon the target reliability of post-construction settlements of FRLTP and DM column-supported embankments.

Each design variable's upper and lower bounds are determined based upon subsoil conditions and constructability issues, which will be described and examined hereafter. The design of the geotechnical structure will be subject to nonlinear constraints per the design code GB/T 50783–2012 (MHURC, 2012). The bearing capacity requirement (ULS) is expressed as:

$$p_z + p_{cz} \le f_{az} \tag{8}$$

where p_z denotes the additional stress induced by surcharge, p_{cz} is the overburden pressure, and f_{az} is the allowable bearing capacity. The piles and the surrounding soil at their tip are deemed a coherent block (or equivalent footing). The bearing capacity is then only related to the soil supporting the pile toe. In contrast, the piles and adjacent soil at the base of the embankment contribute individually to the bearing capacity. This contribution is in two parts, the axial capacity of piles and bearing capacity of the soil, and is given by:

$$q_{az} = \beta_p m \frac{R_a}{A_p} + \beta_s (1-m) f_{sk} \tag{9}$$

where β_p and β_s are the correction factors for the pile and soil, respectively; m denotes the area replacement ratio; R_a is the ultimate axial capacity of a single pile; A_p is the cross-sectional area of pile perpendicular to its vertical axis; f_{sk} is the bearing capacity of the subsoil support. More specifically, the ultimate axial capacity of a single pile R_a is examined by:

$$R_s \le \min[R_{a1}, R_{a2}] \tag{10a}$$

$$R_{a1} = \pi d \sum_{i=1}^{n} q_{si} l_i + \alpha q_p A_p \tag{10b}$$

$$R_{a2} = \eta f_{cu} A_p \tag{10c}$$

where R_s is the axial compressive load on pile head (negative skin friction is also included if any); R_{a1} and R_{a2} are the ultimate axial capacity obtained by the two methods; q_{si} and l_i are the skin friction mobilized at the i^{th} soil layer and corresponding layer thickness; q_p and α are the bearing capacity of subsoil support beneath pile toe and corresponding correction factor; η is the strength reduction factor for piles; f_{cu} is the average of compressive strength of cube specimens with the same mixing ratio as DM columns at 90 days curing.

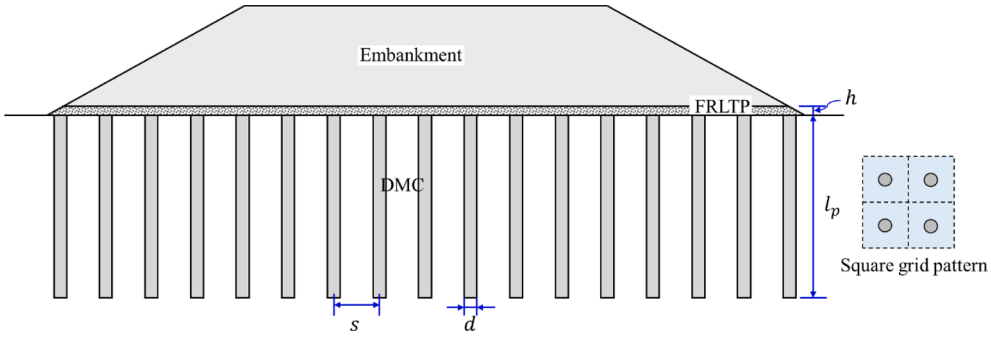

Fig. 14. Structural parameters for basal reinforced DMC-supported embankments (DMC is the deep mixing column; FRLTP is the fiber-reinforced load transfer platform; columns in a square pattern).

Meanwhile, the post-construction settlement is also restricted as per SLS requirements, expressed as:

$$s_{pc} \leq [\Delta s] \tag{11}$$

where s_{pc} is the post-construction settlement and $[\Delta s]$ is the allowable settlement for ensuring the serviceability of the embankment.

Considering all design constraints, the post-construction settlement is the most challenging to obtain, while the rest can be calculated explicitly. The layer-wise summation method and Mindlin stress solution are two widely adopted approaches for calculating the settlement of building foundations. However, some fundamental factors in DM column-supported embankments cannot be assessed by these two methods. Finite element simulation evaluations of the post-construction settlement are performed as an alternative (Sec. 3.1).

4.2. Objective function

The most feasible design in a defined design space may not be unique, meaning additional requirements can be used to find an optimal set of variables considering additional variable(s). Thus, in this study, construction cost optimization is considered using a cost function as the design objective. The design with the minimum construction cost is defined as:

$$\min Q(\boldsymbol{x}) = \widehat{f}(l_p, d, s, h) \tag{12}$$

where $Q(\boldsymbol{x})$ is the cost function, and $\boldsymbol{x} = (l_p, d, s, h)$ is the vector of four design variables. Note that the material and installation costs are closely associated with regional prices and the selection of construction techniques. Therefore, in this study the cost function is determined using specification JTG/T 3832–2018 (MOTPRC, 2018), given by:

$$Q(\boldsymbol{x}) = \frac{c_1 V_{FRLTP} + n c_2 l_p}{a_l} \tag{13}$$

where c_1 and c_2 are the construction costs for FRLTP per cubic meter (c_1 = 3.2 USD/m^3 with the addition of 0.25% fiber) and a single DM column per lineal meter, respectively; V_{FRLTP} is the volume of FRLTP within a transverse dimension of a pile spacing; n is the total number of DM columns along the transverse axis; a_l is the distance in the longitudinal direction.c_2 = 51 USD/m for $l_p \leq 10$ m, and = 59 for $l_p > 10$ m; a correction factor $1.05^{(d-0.5)/0.05}$ is used for c_2 if $d > 0.5$m. Be noted that all costs are approximate and may not fully reflect market conditions.

4.3. Analysis

All feasible design scenarios for a target RI = 1.96 are plotted in Fig. 15, and those yielding the minimum costs for similar settlement conditions are identified and marked red. These data points can be fitted using a logistic function, expressed by

$$s_{post} = \frac{0.61}{1 + \left(\frac{c_{min}}{4625.8}\right)^{5.8}} + 0.3 \tag{14}$$

where s_{post} is the post-construction settlement, and c_{min} is the minimum construction cost per lineal meter of the entire embankment into the page. The original design used in the field is offset from the optimal line, indicating the post-construction settlement and construction cost can both be reduced through design optimization. The threshold is prescribed as the point of maximum curvature (c_{mc}, s_{mc}), wherec_{mc} = 1,275 USD/m ands_{mc} = 0.083 m in this case. The left-hand region of the optimal line (logistic curve) with $c_{min} < c_{mc}$ is defined as cost-effective, while the right side with $c_{min} \geq c_{mc}$ corresponds to the low cost-effective region. More generally, if the control of post-construction settlement $[s_{post}]$ with SLS requirements is smaller than s_{mc}, it is recommended to change the original design to a reinforced foundation using alternative ground improvement techniques, or to modify the type of infrastructure. The optimal design should lie within the range of (s_{mc}, $[s_{post}]$) if $[s_{post}] \rangle s_{mc}$.

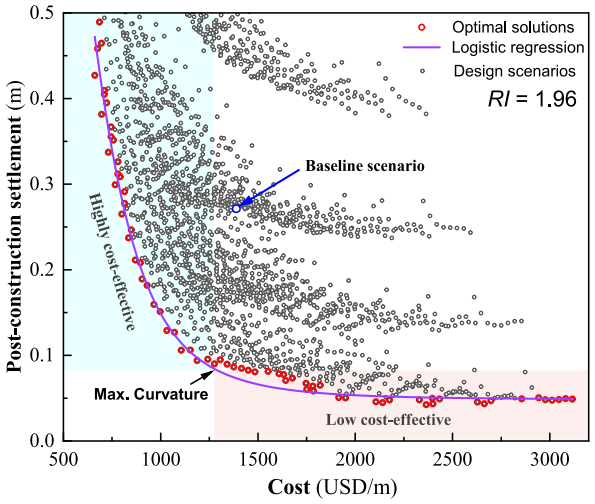

Fig. 15. Design cases and Pareto front of post-construction settlements versus construction costs at RI = 1.96.

Table 4 contains a partial summary of the optimized design variables from the identified optimal data points shown in Fig. 15. Case 15 is the point closest to the point of maximum curvature, corresponding tol_p = 12 m, d = 1.2 m, a = 2.5 m, h = 0.9 m. In most optimal conditions, l_p equals to 12 m because end-bearing piles have much larger bearing capacities than floating piles, resulting in reduced compressive deformation of the underlying problematic soil layers. Increasing the diameter of the piles is also more effective than using closer pile spacing which is consistent with the sensitivity analysis in Fig. 12. A reasonable range of 0.5–0.9 m for the cushion thickness favors the load transfer between pile and soil. For cases where the design variables satisfy both ULS and SLS constraints, the combined use of larger diameter of piles and wider pile spacing is a cost-effective solution. This is because it balances the settlement performance of basal reinforced piled embankments and construction costs.

As displayed in Fig. 16, the optimal lines are obtained by logistic regression for different target reliability levels, RI = 1.0, 1.6, 2.2, and

Table 4
Partial optimized design parameters at RI = 1.96.

Scenario	l_p(m)	d (m)	a (m)	h (m)	s_{post}(m)	c_{min}(USD/m)	Zone
0 (Base)	10.0	1.2	1.9	0.5	0.275	1,388.3	/
1	11.0	0.8	2.5	0.8	0.277	814.2	H
2	12.0	0.8	2.5	0.6	0.264	800.1	H
3	11.0	0.8	2.5	0.9	0.246	848.8	H
4	12.0	0.8	2.5	0.7	0.236	834.8	H
5	12.0	0.8	2.5	0.8	0.210	869.5	H
6	12.0	0.9	2.5	0.7	0.207	895.5	H
7	12.0	0.8	2.5	0.9	0.188	904.1	H
8	12.0	0.9	2.5	0.8	0.181	930.2	H
9	12.0	0.9	2.5	0.9	0.158	964.8	H
10	12.0	1.0	2.5	0.8	0.150	997.1	H
11	12.0	1.0	2.5	0.9	0.128	1,031.8	H
12	12.0	1.1	2.5	0.8	0.126	1,070.9	H
13	12.0	1.1	2.5	0.9	0.105	1,105.5	H
14	12.0	1.2	2.5	0.8	0.105	1,152.2	H
15	12.0	1.2	2.5	0.9	0.093	1,186.9	H
16	12.0	1.3	2.5	0.8	0.095	1,241.9	L
17	12.0	1.3	2.5	0.9	0.089	1,276.5	L
18	12.0	1.4	2.5	0.7	0.094	1,306.1	L
19	12.0	1.4	2.5	0.8	0.089	1,340.7	L
20	12.0	1.4	2.5	0.9	0.086	1,375.4	L

Note: H, highly cost-effective; L, low cost-effective.

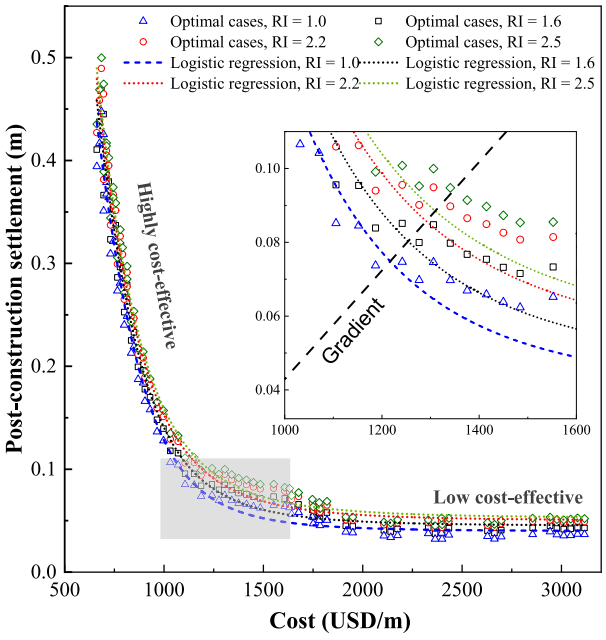

Fig. 16. Pareto fronts with different reliability levels of settlements.

2.5. All optimal curves show a similar trend, and thresholds can be determined by calculating the points of maximum curvature. A linear relationship is observed between s_{mc} (cm) and target reliability index RI,

$$s_{mc} = 1.2RI + 5.89 \tag{15}$$

Eq. (15) can be used to approximate the range of post-construction settlement expected for the cost-effective designs explored, and serves as a reference for deciding whether alternative ground improvement techniques should be employed.

5. Discussion

The proposed method exhibits potential for conducting reliability assessments of piled embankments coupled with economic evaluations, thereby assisting project decision-making, as demonstrated by the case study. Nevertheless, careful attention must be paid to the following aspects when implementing this method.

The case study utilizes 2D FEM models to analyze post-construction settlements. Previous research (Chai et al., 2015) found that the 2D model can accurately predict ground settlement and excess pore pressure dissipation in soft clay under embankment loading. However, it may be less reliable in determining column bending moments and lateral ground movement beneath embankment slope toe compared to 3D models. Despite this, the calculated settlements from the 2D models are used primarily as inputs for structural optimization, rendering them acceptable. Nonetheless, it is crucial to address potential errors in specific scenarios, particularly when lateral ground movement and column bending moments are adopted as indicators in the embankment design.

Soil creep behavior is not considered in the FEM models for settlement analysis. Primary consolidation is usually more impactful than secondary consolidation, but ignoring secondary consolidation can be problematic when settlement rates are high and the consolidation process continues over a prolonged period, especially in organic clays and sensitive clays. Although the measured settlement over time in Fig. 5 shows insignificant soil creep in this study, it is essential to adequately characterize soil creep behavior for uncertainty modeling of embankment settlements depending on the specific soil types, environmental factors, and stress conditions present.

The case study focuses solely on incorporating the soil constitutive parameters as random variables in the uncertainty modeling, to showcase the proposed modeling framework. However, for investigating time-dependent ground behavior under embankment loading, there is potential for further analysis of additional parameter variations, such as creep index and pre-consolidation of soft clay, as well as column properties.

The uncertainty of MCC constitutive parameters in the case study was linked solely to the soil plastic index using the NN-MCD algorithm. While this estimation proved effective and utilized well-documented experimental data inputs, it is important to recognize that material properties are influenced by numerous factors. Disregarding the effects of soil state and structure in determining κ could result in unanticipated biased estimates. Therefore, it is crucial to employ alternative approaches or comprehensive databases to accurately assess and address these potential errors.

Assessing the economic viability of DM columned embankments is a multifaceted challenge, yet the presented case study offers a simplified perspective. To effectively design DM columns for ground improvement initiatives, several factors must be taken into account, such as the soil type, intended use of the improved ground, and load requirements. The costs of constructing DM columns are contingent upon site investigation, design parameters, selection of appropriate mixing equipment, and a quality control program. Thus, inclusion of these variables in the economic assessment model is crucial to ensuring the practicality of the projected outcomes. When the number of factor inputs is high, exhaustive search becomes impractical for structural optimization, and advanced optimization algorithms (Chen et al., 2021) should be used instead to facilitate decision-making.

In addition, constructing columned embankments can be economically viable if the long-term costs of maintaining the geo-structure are taken into account. Evaluating the total cost of the project over its lifespan, by including whole-of-life maintenance in the economic assessment, can identify the most cost-effective design and construction options that minimize long-term maintenance costs. For instance, settlement can be substantially reduced with relatively low-cost measures (Fig. 15), leading to significant savings in maintenance costs over the pavement's lifespan. To make informed decisions regarding the use of deep mixing columns, future investigations should explore performing cost-benefit analyses before a comprehensive reliability assessment of columned embankments.

6. Conclusions

A novel hybrid modeling framework was developed to simulate the long-term settlements of basal reinforced piled embankment (BRPE) systems. The mathematical model and optimization problem were described by identifying structural components, fundamental design variables, design constraints including ULS and SLS requirements, and an objective function related to construction costs. The settlement-based optimization was conducted to obtain optimal design that satisfied the constraints while giving the minimum construction cost and meting the target settlement reliability level.

The NN-MCD algorithm can predict strength-related Modified Cam-Clay model parameters (critical state ratio M, the isotropic swelling index κ) based on an experimental dataset of soil plasticity index, with results obeying a normal distribution instead of producing a single value. Coupled FE analysis using the constitutive parameters of soil generated by NN-MCD allows for the uncertainty analysis of long-term deformation behavior for assessing BRPE performance, agreeing with monitoring results.

The designed BPNN architecture with double input layers is suitable for surrogate modeling. The integration of the BPNN-based surrogate model and FE analysis can efficiently obtain the post-construction settlements of BRPEs in any design scenario using a limited number of training samples. In the application, the proposed settlement-oriented cost optimization technique avoids incorporating any complex gradient-based optimization method and is easy to interpret. In optimal

design scenarios, the Pareto fronts can be well captured by the logistic functions at any target reliability level (settlement). A threshold is suggested to be located at the maximum curvature of the fitting curve, defining two zones whether the design is highly or low cost-effective. The ground modification technique should be modified (use of BRPE may not satisfy economic feasibility) if the optimized system corresponds to a low cost-effective solution.

The proposed hybrid framework balances computational effort and accuracy. It can be extended to examine the variability of additional critical parameters (e.g. over-consolidation ratio, hydraulic conductivity, initial structure, and creep index) and their impacts on the development of embankment settlements. In addition, the presented work shows excellent potential to analyze similar engineering-scale optimization problems while conducting risk evaluation.

CRediT authorship contribution statement

Tengfei Wang: Conceptualization, Funding acquisition, Writing – original draft, Supervision. **Weihang Chen:** Formal analysis, Investigation, Software. **Taifeng Li:** Resources, Project administration, Funding acquisition. **David P. Connolly:** Writing – review & editing. **Qiang Luo:** Funding acquisition, Project administration. **Kaiwen Liu:** Resources. **Wensheng Zhang:** Validation.

Declaration of Competing Interest

The authors declare that they have no known competing financial interests or personal relationships that could have appeared to influence the work reported in this paper.

Data availability

Data will be made available on request.

Acknowledgments

This work was supported by the National Natural Science Foundation of China (grant No. 52078435), the Technology Research and Development Plan Program of China National Railway Group Limited (grant No. P2021G053), the Natural Science Foundation of Sichuan Province (grant Nos. 2023NSFSC0391 and 2022NSFSC0404), and the Foundation of China Academy of Railway Sciences Co., Ltd. (grant No. 2021YJ071).

References

Akio, N., Takeshi, K., Osamu, K., 1988. Constitutive Parameters Estimated by Plasticity Index. J. Geotech. Eng. 114, 844–858.

Alibeikloo, M., Khabbaz, H., Fatahi, B., 2022. Random Field Reliability Analysis for Time-Dependent Behaviour of Soft Soils Considering Spatial Variability of Elastic Visco-Plastic Parameters. Reliab. Eng. Syst. Saf. 219, 108254 https://doi.org/10.1016/j.ress.2021.108254.

Alkhorshid, N.R., Araujo, G.L.S., Palmeira, E.M., 2021. Consolidation of soft clay foundation improved by geosynthetic-reinforced granular columns: Numerical evaluation. J. Rock Mech. Geotech. Eng. 13, 1173–1181. https://doi.org/10.1016/j.jrmge.2021.03.004.

Burland, J.B., 1990. On the compressibility and shear strength of natural clays. Géotechnique 40, 329–378. https://doi.org/10.1680/geot.1990.40.3.329.

Chai, J.C., Shrestha, S., Hino, T., Ding, W.Q., Kamo, Y., Carter, J., 2015. 2D and 3D analyses of an embankment on clay improved by soil-cement columns. Comput. Geotech. 68, 28–37.

Chai, J., Shrestha, S., Hino, T., Uchikoshi, T., 2017. Predicting bending failure of CDM columns under embankment loading. Comput. Geotech. 91, 169–178. https://doi.org/10.1016/j.compgeo.2017.07.015.

Chen, C., Mao, F., Zhang, G., Huang, J., Zornberg, J. g., Liang, X., Chen, J., 2021. Settlement-based cost optimization of geogrid-reinforced pile-supported foundation. Geosynthetics International 28, 541–557. 10.1680/jgein.21.00002.

Chen, W., Luo, Q., Liu, J., Wang, T., Wang, L., 2022. Modeling of frozen soil-structure interface shear behavior by supervised deep learning. Cold Reg. Sci. Technol. 200, 103589 https://doi.org/10.1016/j.coldregions.2022.103589.

Dang, C., Dang, L., Khabbaz, H., Sheng, D., 2021. Numerical Study on Deformation Characteristics of Fibre Reinforced Load Transfer Platform and Columns Supported Embankments. Can. Geotech. J. 58, 328–350. https://doi.org/10.1139/cgj-2019-0401.

Gal, Y., Ghahramani, Z., 2016. Dropout as a Bayesian approximation: representing model uncertainty in deep learning. International Conference on Machine Learning. 1050–1059.

Guo, X., Pham, T.A., Dias, D., 2023. Multi-objective optimization of geosynthetic-reinforced and pile-supported embankments. Acta Geotech. https://doi.org/10.1007/s11440-022-01782-4.

He, X., Xu, H., Sabetamal, H., Sheng, D., 2020. Machine learning aided stochastic reliability analysis of spatially variable slopes. Comput. Geotech. 126, 103711 https://doi.org/10.1016/j.compgeo.2020.103711.

He, X., Wang, F., Li, W., Sheng, D., 2021. Efficient reliability analysis considering uncertainty in random field parameters: Trained neural networks as surrogate models. Comput. Geotech. 136, 104212 https://doi.org/10.1016/j.compgeo.2021.104212.

He, X., Wang, F., Li, W., Sheng, D., 2022. Deep learning for efficient stochastic analysis with spatial variability. Acta Geotech. 17, 1031–1051. https://doi.org/10.1007/s11440-021-01335-1.

Jamsawang, P., Yoobanpot, N., Thanasisathit, N., Voottipruex, P., Jongpradist, P., 2016. Three-dimensional numerical analysis of a DCM column-supported highway embankment. Comput. Geotech. 72, 42–56. https://doi.org/10.1016/j.compgeo.2015.11.006.

Karstunen, M., Rezania, M., Sivasithamparam, N., Yin, Z.Y., 2015. Comparison of Anisotropic Rate-Dependent Models for Modeling Consolidation of Soft Clays. Int. J. Geomech. 15, A4014003. https://doi.org/10.1061/(ASCE)GM.1943-5622.0000267.

Karstunen, M., Yin, Z.-Y., 2010. Modelling time-dependent behaviour of Murro test embankment. Géotechnique 60, 735–749. https://doi.org/10.1680/geot.8.P.027.

Kendall, A., Gal, Y., 2017. What Uncertainties Do We Need in Bayesian Deep Learning for Computer Vision?, in: Proceedings of the 31st International Conference on Neural Information Processing Systems, NIPS'17. Curran Associates Inc., Red Hook, NY, USA, pp. 5580–5590.

Ling, Z., Shuai, Z., Heng, Z., 2021. Coupling-Based Elastic Solution of Arching Evolution for GRPSE. J. Eng. Mech. 147, 6021005. https://doi.org/10.1061/(ASCE)EM.1943-7889.0001994.

Liu, H.Y., Luo, Q., El Naggar, M.H., Zhang, L., Wang, T.F., 2023. Centrifuge modeling of stability of embankment on soft soil improved by rigid columns. J. Geotech. Geoenviron. Eng. https://doi.org/10.1061/JGGEFK.GTENG-11314.

Liu, K., Rowe, R.K., 2015. Numerical modelling of prefabricated vertical drains and surcharge on reinforced floating column-supported embankment behaviour. Geotext. Geomembr. 43, 493–505. https://doi.org/10.1016/j.geotexmem.2015.05.006.

Ma, H., Luo, Q., Wang, T., et al., 2021. Numerical stability analysis of piled embankments reinforced with ground beams. Transp. Geotech. 26, 100427.

Mašín, D., 2015. The influence of experimental and sampling uncertainties on the probability of unsatisfactory performance in geotechnical applications. Géotechnique 65, 897–910. https://doi.org/10.1680/jgeot.14.P.161.

MHURC, 2012. Technical Code for Composite Foundation. China Planning Press, Beijing, China.

MOHURD, 2019. GB 50216-2019 Unified Standard for Reliability Design of Railway Structures. China Planning Press, Beijing.

MOTPRC, 2018. Highway engineering quota and budget. China Communication Press Co., Ltd., Beijing, China.

Nguyen, V.D., Luo, Q., Wang, T., et al., 2022. Monitoring of an instrumented geosynthetic-reinforced piled embankment with a triangular pile configuration. Int. J. Rail Transp. 11 (1), 69–91.

Nguyen, V.D., Luo, Q., Wang, T., et al., 2023. Load Transfer in Geosynthetic-Reinforced Piled Embankments with a Triangular Arrangement of Piles. J. Geotech. Geoenviron. Eng. 149 (2), 04022131.

Okyay, U.S., Dias, D., 2010. Use of lime and cement treated soils as pile supported load transfer platform. Eng. Geol. 114, 34–44. https://doi.org/10.1016/j.enggeo.2010.03.008.

Pham, T.A., Guo, X., Dias, D., 2022. Internal stability analysis of column-supported embankments: Deterministic and probabilistic approaches. Transp. Geotech. 37, 100868 https://doi.org/10.1016/j.trgeo.2022.100868.

Phutthananon, C., Jongpradist, P., Jongpradist, P., Dias, D., Jamsawang, P., Bergado, D. T., 2021. Performance-based design optimization of embankments resting on soft soil improved with T-shaped and conventional DCM columns. Acta Geotech. 16, 3301–3326. https://doi.org/10.1007/s11440-021-01258-x.

Rumelhart, D.E., Hinton, G.E., Williams, R.J., 1986. Learning representations by back-propagating errors. Nature 323, 533–536. https://doi.org/10.1038/323533a0.

Taylor, D.W., 1948. Fundamentals of Soil Mechanics. Chapman And Hall, Limited, New York.

Vivi, A., Asadi, A., Huat, B.B.K., Haslinda, N., 2015. Performance of Chemically Treated Natural Fibres and Lime in Soft Soil for the Utilisation as Pile-Supported Earth Platform. Int. J. Geosyn. Ground Eng. 1, 1–14.

Wang, T., Ma, H., Liu, J., Luo, Q., Wang, Q., Zhan, Y., 2021. Assessing frost heave susceptibility of gravelly soils based on multivariate adaptive regression splines model. Cold Reg. Sci. Technol. 181, 103182 https://doi.org/10.1016/j.coldregions.2020.103182.

Wang, T., Nguyen, V.D., Bui, P.D., Luo, Q., Liu, K., Zhang, L., 2023. Three-dimensional physical modeling of load transfer in basal reinforced embankments under differential settlement. Geotext. Geomembr. 51 (2), 330–341.

Wu, L., Jiang, G., Ju, N., 2019b. Behavior and Numerical Evaluation of Cement-Fly Ash-Gravel Pile-Supported Embankments over Completely Decomposed Granite Soils. Int. J. Geomech. 19, 04019048. https://doi.org/10.1061/(ASCE)GM.1943-5622.0001430.

Wu, J.T., Ye, X., Li, J., Li, G.W., 2019a. Field and numerical studies on the performance of high embankment built on soft soil reinforced with PHC piles. Comput. Geotech. 107, 1–13. https://doi.org/10.1016/j.compgeo.2018.11.019.

Yang, Y.-J., Li, D.-Q., Cao, Z.-J., Gao, G.-H., Phoon, K.-K., 2021. Geotechnical reliability-based design using generalized subset simulation with a design response vector. Comput. Geotech. 139, 104392 https://doi.org/10.1016/j.compgeo.2021.104392.

Yapage, N.N.S., Liyanapathirana, D.S., 2014. A parametric study of geosynthetic-reinforced column-supported embankments. Geosynth. Int. 21, 213–232. https://doi.org/10.1680/gein.14.00010.

Yoobanpot, N., Jamsawang, P., Krairan, K., Jongpradist, P., Likitlersuang, S., 2020. Laboratory investigation of the properties of cement fly ash gravel for use as a column-supported embankment. Constr. Build. Mater. 257, 119493 https://doi.org/10.1016/j.conbuildmat.2020.119493.

Yoon, G.L., Kim, B.T., Jeon, S.S., 2004. Empirical correlations of compression index for marine clay from regression analysis. Can. Geotech. J. 41, 1213–1221. https://doi.org/10.1139/t04-057.

Zhang, Z., G., Y., Cai, Y., Zhang, Z., 2019. Centrifugal and numerical modeling of stiffened deep mixed column-supported embankment with slab over soft clay. Canad. Geotech. J. 56, 1418–1432. 10.1139/cgj-2018-0180.

Zhang, P., Jin, Y.-F., Yin, Z.-Y., 2021b. Machine learning–based uncertainty modelling of mechanical properties of soft clays relating to time-dependent behavior and its application. Int. J. Numer. Anal. Meth. Geomech. 45, 1588–1602. https://doi.org/10.1002/nag.3215.

Zhang, L., Wang, L., Zhou, A., Xu, Y., Xia, X., 2021a. Semi-analytical solutions to the consolidation of unsaturated composite ground enforced by stone columns under equal strain condition considering smear effect. Transp. Geotech. 31, 100644 https://doi.org/10.1016/j.trgeo.2021.100644.

Zhang, R., Wu, C., Goh, A.T.C., Böhlke, T., Zhang, W., 2021d. Estimation of diaphragm wall deflections for deep braced excavation in anisotropic clays using ensemble learning. Geosci. Front. 12, 365–373. https://doi.org/10.1016/j.gsf.2020.03.003.

Zhang, P., Yin, Z.-Y., Jin, Y.-F., Chan, T.H.T., Gao, F.-P., 2021c. Intelligent modelling of clay compressibility using hybrid meta-heuristic and machine learning algorithms. Geosci. Front. 12, 441–452. https://doi.org/10.1016/j.gsf.2020.02.014.

Zhang, P., Yin, Z.-Y., Jin, Y.-F., 2022. Bayesian neural network-based uncertainty modelling: application to soil compressibility and undrained shear strength prediction. Can. Geotech. J. 59, 546–557. https://doi.org/10.1139/cgj-2020-0751.

Zhang, D., Zhang, Y., Kim, C.W., Meng, Y., Garg, A., Garg, A., Fang, K., 2018. Effectiveness of CFG pile-slab structure on soft soil for supporting high-speed railway embankment. Soils Found. 58, 1458–1475. https://doi.org/10.1016/j.sandf.2018.08.007.

Zheng, G., Yu, X., Zhou, H., Wang, S., Zhao, J., He, X., Yang, X., 2020. Stability analysis of stone column-supported and geosynthetic-reinforced embankments on soft ground. Geotext. Geomembr. 48, 349–356. https://doi.org/10.1016/j.geotexmem.2019.12.006.

Zhou, M., Liu, H., Chen, Y., Hu, Y., 2016. First application of cast-in-place concrete large-diameter pipe (PCC) pile-reinforced railway foundation: a field study. Can. Geotech. J. 53, 708–716.